World Conference on
Timber Engineering
Oslo 2023

A 3D DUCTILE-NOTCHED CONNECTION FOR TIMBER-CONCRETE COMPOSITE BEAM : EXPERIMENTAL INVESTIGATION

Adham Al Rahim[1], Piseth Heng[2], Clemence Lepourry[3], Hugues Somja[4], Franck Palas[5]

ABSTRACT: A 3D ductile-notched connection for timber concrete composite beams is proposed in this study. The innovation of the proposed connector is the particular geometry of the notch. This configuration on one hand generates three shear planes instead of one as typical notched connection and on the other hand provides a mechanical locking to limit the uplift without the need for metallic screws. This paper presents an experimental investigation on the behaviour of the newly proposed notched connector. Three pushout tests were performed. The results show high strength and stiffness as well as ductility, as the failure mode was governed by local crashing of the timber. In addition, one flexural test was carried out on the beam specimen. The mode of failure was governed by flexural failure of the timber beam. The analysis of the slip and the uplift demonstrated the effectiveness of the connectors.

KEYWORDS: 3d ductile-notched connection, Timber-concrete composite beam, Pushout tests, Inversed flexural tests

1 INTRODUCTION

The new environmental regulations such as the RE2020 [1] in France stimulate the interest of using structural timbers in the construction within the last few years. However, timber slabs fulfil hardly all the criteria for serviceability. In this case, timber-concrete composite members represent a great compromise by associating timber with concrete. This association can improve the flexural strength and stiffness of the members as well as the sound insulation, the vibration performance, and the thermal insulation properties [2]. Several configurations of shear connectors have been proposed for timber-concrete composite members [3]. For instance, ordinary smooth nails of 70 mm with a diameter of 3.4 mm, arranged in pair, have been used as timber-concrete connectors [4]. 12 mm and 16 mm lag screws have been employed for their hybrid failure mode related to the steel's plastic deformation [5]. The first research on tooth plates was conducted in 1984. This technology was used in the construction of timber-concrete composite wall in Sweden [6]. The use of adhesive and epoxy resin within the connection system has been also investigated [7]. Although notched connections perform well in term of strength and stiffness, poor ductility is obtained when the failure is governed by shear rupture of the concrete notch [8]. Steel screws placed inside the concrete notches are sometimes added to improve the post-peak behaviour [9], but the installation of these steel fasteners increases the construction cost. In this context, a novel composite floor technology, called Bobé, is proposed (see Figure 1a). It combines a reinforced concrete slab and an inverted T-shaped wooden beam, which are joined by means of 3D notch connectors with three shear planes. The particular shape of the notch provides a geometrical locking for limiting the uplift, and the rebars (Figure 1b) improve the post-peak behaviour of the connection.

This paper presents an experimental study on the behaviour of the proposed notched connectors for timber-concrete composite beams. In this study, a series of three symmetrical pushout tests were performed in order to determine the strength, stiffness, ductility and failure of the connection system. In addition, a six-point bending test has been made to verify the effectiveness of the notched connection for timber-concrete composite beams.

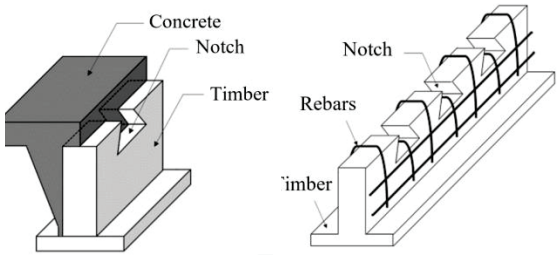

Figure 1: *3D notched connectors for timber-concrete beams.*

[1] Adham Al Rahim, LGCGM/Structural Engineering Research Group, INSA de Rennes, France, adham.al-rahim@insa-rennes.fr
[2] Piseth Heng, LGCGM/Structural Engineering Research Group, INSA de Rennes, France, piseth.heng@insa-rennes.fr
[3] Clemence Lepourry, INGENOVA, France, clemence.lepourry@ingenova-lab.fr
[4] Hugues Somja, LGCGM/Structural Engineering Research Group, INSA de Rennes, France, hugues.somja@insa-rennes.fr
[5] Franck Palas, Concept Technique Design R & D, France, franck.palas@ctdconseils.com

https://doi.org/10.52202/069179-0435

2 PUSHOUT TESTS

2.1 SPECIMENS AND TEST SETUP

The pushout test program included three identical specimens, noted by S1, S2 and S3. The specimens are made of two glued timber panels of solid pine (Spruce) with a grade of C24, measuring 1020 mm in height, 360 mm in width, and 70 mm in thickness, embedded between two concrete slabs (see Figure 2a). The compressive strength of timber, has been tested on 10 compressive pieces, parallel to the grain, with a cross section of 75 x 200 mm and length of 450 mm, according to EN 408 guideline [10]. An average resistance of 34.30 MPa, with a standard deviation of 3.19 MPa, was obtained. The average moisture content was found to be 13.05%, with a standard deviation of 1.27%.

Regarding the pushout specimens, two shear connectors, with a spacing of 326 mm, are made on each timber panel, as illustrated in Figure 2b. The concrete slabs were 450 mm in width, 1120 mm in length, and 80 mm in thickness (Figure 2c). The concrete strength grade was C25/30. The real average strength, obtained from compressive tests on cylindrical specimens, with a diameter of 110 mm and a length of 220 mm, was 27.7 MPa, with a standard deviation of 1.58 MPa. In turn, the notches are reinforced with B500B grade U-shaped rebars, with a diameter of 6 mm.

In order to reduce the friction, and to ensure a smooth contact between the materials, the timber panels were painted before concrete casting. For all specimens, the first of the two concrete slabs were cast on the same day in a horizontal position. Two days after, the specimens were lifted and turned over for the second casting. The timber panel and concrete slabs had an offset of 100 mm in length.

The test setup is described in Figure 3a. The compression load is imparted on the wooden panel by means of a hydraulic jack with 1000 kN capacity and a stroke length of 200 mm, and transferred to the concrete slabs through the connectors. Subsequently, the load is counterbalanced by the reaction forces provided by the rigid supporting system.

The monotonic loading protocol, derived from EN 26891, started with an initial ramp up to 40% of the estimated failure load, followed by a discharge and then a steady increase up to failure. The estimated capacity (F_{est}) of the specimen, with four connectors, was estimated to be 188 kN referring to the BNTEC guidelines [12]. The loading is sustained until the specimen failure is reached.

The measurement devices for the push out tests are illustrated in Figure 3b. The relative slip and uplift between timber and concrete were recorded by linear variable displacement transducers (LVDTs). On each side of the specimen, four uplift LVDTs with a stroke length of 2.5 mm and 6 mm, and four slip LVDTs with a stroke length of 25 mm, were attached.

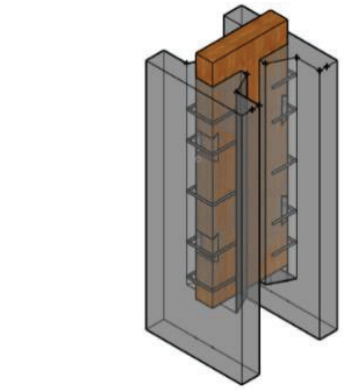

(a).

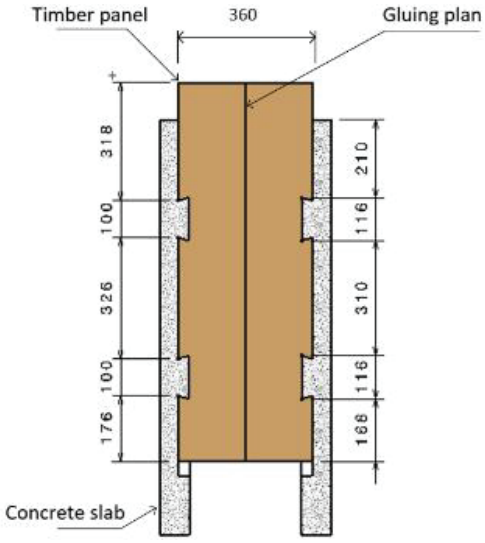

(b).

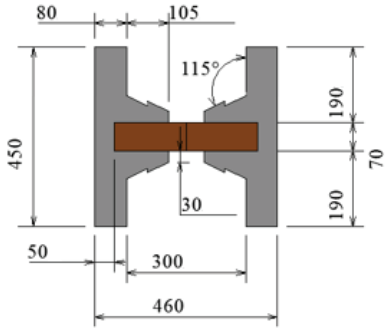

(c).

Figure 2: *(a) 3D view. (b) Front view. (c) Top view.*

https://doi.org/10.52202/069179-0435

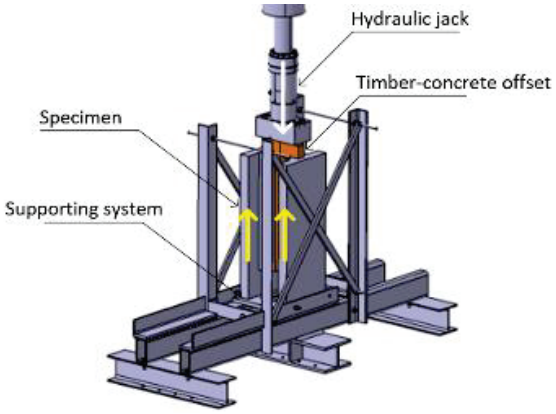

(a).

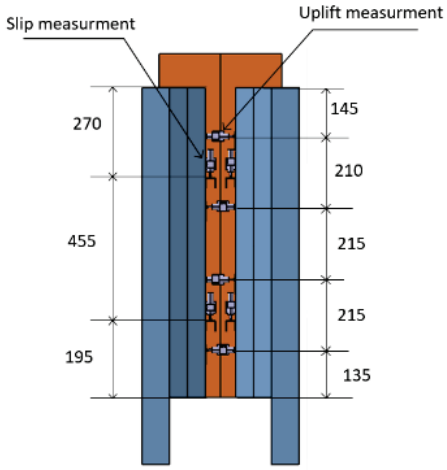

(b).

Figure 3: *(a) Test setup. (b) Measurement devices.*

2.2 RESULTS

Figure 4a and Figure 4b exhibit the evolution of the applied force as a function of the mean slip and the mean uplift, respectively. A high ductility of the connection was obtained, as the failure mode in the three tests was governed by the local crushing of the timber. The specimens were cut after tests to allow for an assessment of large compressive deformation of timber at the position of the notch connections (Figure 5). The maximum forces (F_{max}) obtained are 206.8 kN, 170.1 kN, and 198.5 kN for tests S1, S2 and S3, respectively. Adopting the method proposed by Ceccotti [13], the mean stiffness at serviceability limit state (K_s) and at ultimate limit state (K_u) are 184.8 kN/mm with a standard deviation of 19.3 kN/mm and 167.3 kN/mm with a standard deviation of 15.5 KN/mm, respectively.

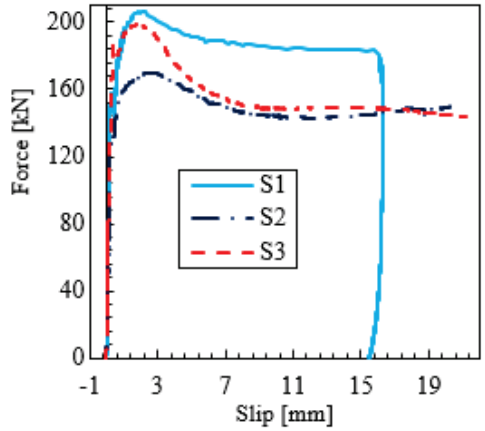

(a).

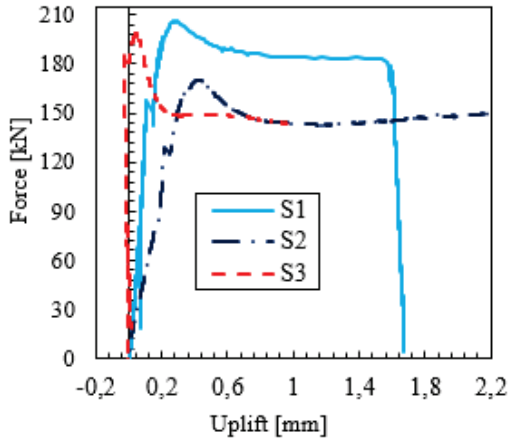

(b).

Figure 4: *(a) Force-slip curves. (b) Force-uplift curves.*

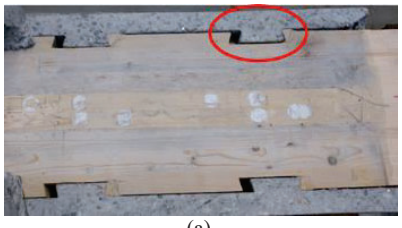

(a).

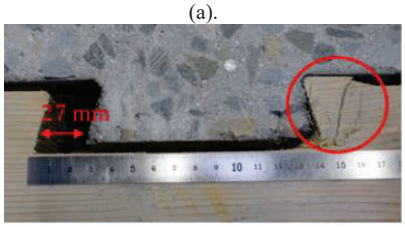

(b).

Figure 5: *(a) Local crushing of timber. (b) Zoom version.*

3 SIX-POINT BENDING TEST

3.1 SPECIMENS AND TEST SETUP

This test aims at studying the flexural behaviour of the timbre-concrete floor system.

Three specimens of the timber concrete composite beam, noted F_1, F_2, and F_3, were designed and fabricated. Each specimen was made of two identical T-shape wooden beams connected to a concrete slab using 14-notched connectors, with a spacing of 426 mm (Figure 7a). The T beam, had a cross section of 175 x 68 mm (height x width) for the web and 58 x 145 mm (height x width) for the flange (Figure 7b). For reducing friction between materials and ensure a smooth interface, the timber beams were coated with paint before concrete casting. The average moisture content in timber beams of the specimens was measured before flexural tests of F_1, F_2, and F_3, at 8%, 9%, and 8%, respectively.

To determine the mechanical properties of the timber beams, ten wooden pieces, with a mean cross section of 68 x 173 mm and a mean length of 397 mm, were tested for their compressive strength parallel to the grain. The average compressive modulus of elasticity (MOE) was 5297 MPa, with a standard deviation of 834 MPa. The flexural modulus of elasticity, tested on ten timber beams at the measured moisture content, was 11166 MPa with a standard deviation of 1445 MPa [14].

The timber beams were embedded in the concrete slab with an insertion depth of 20 mm. The concrete slab was designed with dimensions of 6845 x 920 x 80 mm (length x width x thickness) (see Figure 7b). The concrete slab was reinforced with a rebar mesh ST10 with a rebar diameter of 6 mm and a spacing of 200 mm. The actual average concrete strength was determined on cylindrical samples of 110 x 220 mm (diameter x length), on the same day of each flexural test. The results were 25.26 MPa (27 days age), 47.81 MPa (43 days age), and 23.26 MPa (92 days age), with a standard deviation of 0.124 MPa, 3.25 MPa, and 2.92 MPa, for F_1, F_2, and F_3, respectively.

The test setup consisted of a 1500 kN capacity hydraulic jack, a guidance system for a vertical loading only, two supporting systems, and a spreading system to transfer the applied load to the specimen through four points (Figure 7c).

The flexural performances were investigated via a reversed six-point bending test. In such a configuration, the specimen is invertedly mounted on the testing device, and a vertical pull is exerted by the hydraulic jack (Figure 7a). This specific setup has been developed in order to obtain measurements for loads lower than the weight of the specimen.

For all three specimens, the same loading protocol was respected. It consists of five consecutive phases (Figure 7b): 1. Lifting of the specimen upon contact with the supports, 2. Assembly of the lag screws between the supporting system and the specimen, 3. Quasi-permanent service limit state (SLS) cycling (five to seven cycles), 4. Ultimate limit state (ULS) cycling (one cycle), and 5. Loading to the failure. Service and ultimate limit states correspond to the loads of use category A (floors) in Eurocode 1 [15].

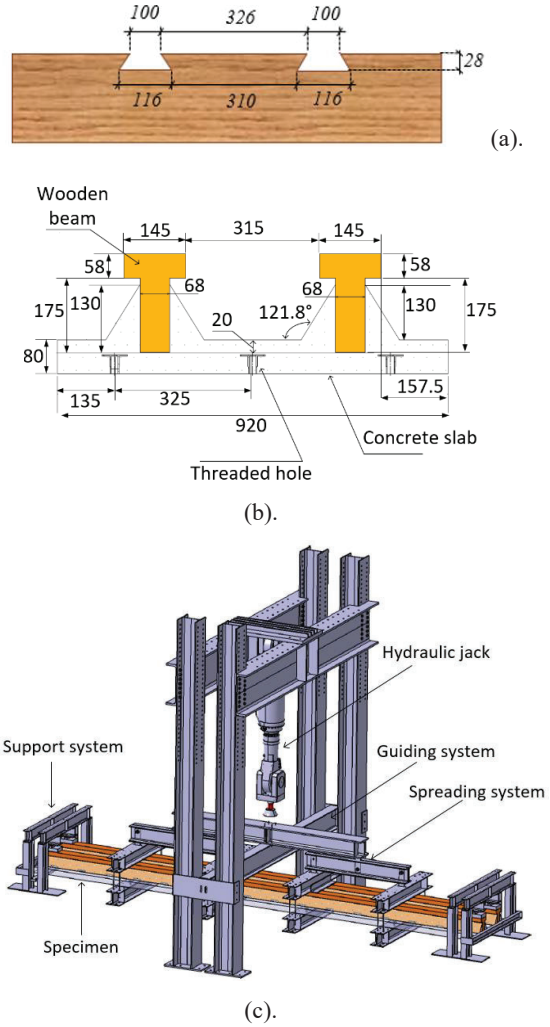

Figure 6: *(a) Notch connectors geometry and spacing. (b) Cross section dimensions of timber concrete floor. (c) 3D test setup. Dimensions in mm.*

Before the test began, the specimen was lifted slowly to make contact with the supports. During this phase, the accuracy of the instrument's operation and data acquisition was checked. Once contact was achieved, the test officially started. A displacement control was adopted, with a speed of 3 mm/min.

To measure the interface slips between the timber and concrete, eighteen linear variable differential transducers (LVDTs) were fixed horizontally on the timber beams with nine being located on front side and nine on the back side of the specimen. For the uplift, ten LVDTs were attached vertically on the timber beams. Five LVDTs were affixed to the front side of the specimen and another five were fixed on the back of the specimen. For both measurements, the pushrod of LVDT was set in contact with a steel plate that was glued on the concrete side. Additionally, five LVDTs are employed to quantify the vertical deflection of the specimen (Figure 8).

https://doi.org/10.52202/069179-0435

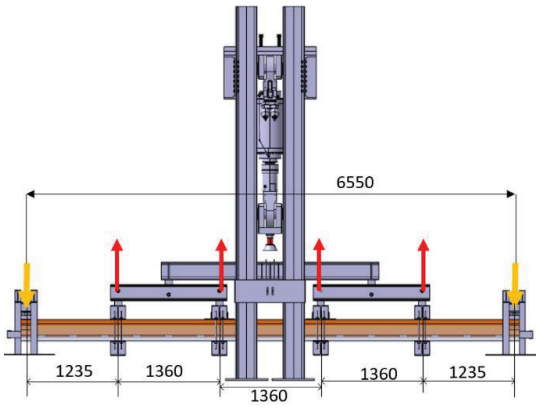

(a).

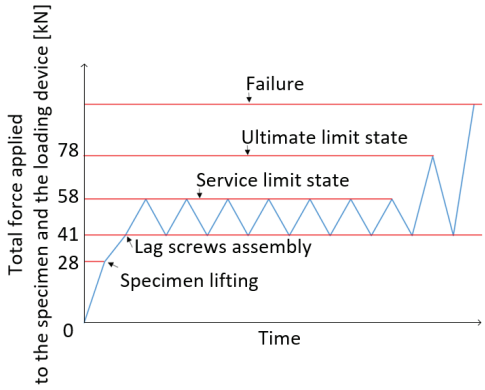

(b).

Figure 7: *(a) 2D test setup. (b) Protocol. Dimensions in mm.*

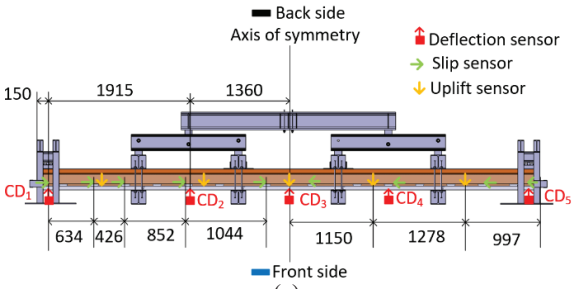

(a).

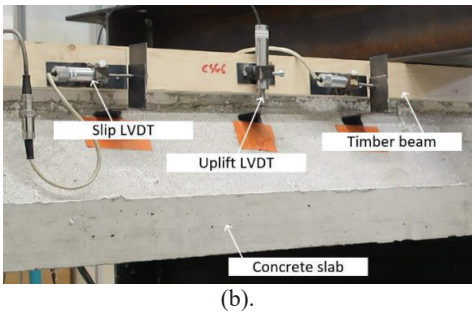

(b).

Figure 8: *(a). Bending test instrumentation. (b). Reel photo of instrumentation.*

3.2 TEST RESULTS

3.2.1 Load capacity and failure mode

In the initial period of loading, at the service limit state compaction, there was no visible cracks in timber beams or concrete slab of the specimens F_1 and F_2, while, some cracks were observed on the concrete drop in the specimen F_3 (see Figure 10a). At the ultimate limit state, as the load was on the increase, invisible fibre breakage of wood were heard and fractures appeared on the concrete drop of F_1, F_2, and F_3. During the loading process to the total collapse, failure occurred at mid-span due to the combination of bending and tensile fractures in the flange of the timber beam. The collapse of F_1, F_2, and F_3 was governed by the rupture of the timber beam (see Figure 10b, Figure 10c, and Figure 10d). The maximum loads reached were 130.2 kN, 123.5 kN, and 128 kN, applied on F_1, F_2 and F_3, respectively. The corresponding mid-span deflection was 61 mm, 47.2 mm, and 68.6 mm, respectively (Figure 9).

However, the examination after collapse uncovered the absence of shear failure at the locations of timber-concrete connectors for all specimens tested. In addition, the uplifts between the concrete and the timber were limited, demonstrating the excellent shear resistance exhibited by the selected connectors.

3.2.2 Experimental bending stiffness

Figure 9 displays the force vs mid-span deflection curves for all the specimens. The experimental bending stiffness was calculated by Eq. (1) based on the elementary beam theory.

$$EI_{exp} = \frac{F}{4w}\left[\frac{1}{2}(2a+b)\left(a+\frac{3}{2}b\right)^2\right] \quad (1)$$

In such expression, a is the distance from the loading point to the support, a = 1235 mm; b is the distance between two loading points, b = 1360 mm; F is the maximum force applied by the hydraulic jack to the specimen during the compaction cycle; w is the corresponding mid-span deflection.

The results of the three tests are collected in the Table *1*.

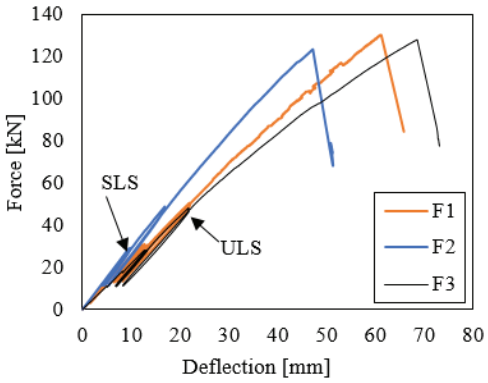

Figure 9: *Load-deflection curves at mid-span of all specimens.*

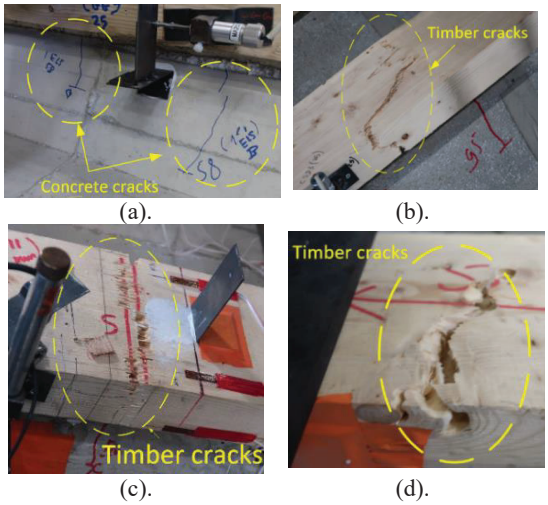

(a). (b). (c). (d).

Figure 10: *(a). Cracks in concrete drop. (b). Failure of F_1. (c). Failure of F_2. (d). Failure of F_3.*

Table 1 Flexural rigidity of the test specimens.

Specimen	$\mathbf{EI_{1-SLS}}$ (10^{13}) Nmm^2	$\mathbf{EI_{ULS}}$ (10^{13}) Nmm^2
F_1	1.22	1.15
F_2	1.57	1.49
F_3	1.14	1.13

Where, EI_{1-SLS} is the flexural rigidity at the 1st cycle of the service limit state, and EI_{ULS} is the flexural rigidity at the ultimate limit state. It can be observed that the flexural stiffness of specimens F_1 and F_3 exhibit a comparable level, while that of the specimen F_2 is relatively higher. The higher concrete strength measured in the F_2 test might be a contributing factor.

3.2.3 Relative slip

The relative slips along the composite beam span were depicted in Figure 11 at different load levels. The three cases have shown the higher relative slips occurred at the both ends of the beam. The maximum relative slips were 0.72 mm, 0.92 mm, and 1.98 mm, recorded for F_1, F_2, and F_3, respectively. However, the relative slips obtained from the bending test do not exceed the plastic resistance of the connector obtained in push-out tests (see Figure 4a).

3.2.4 Interface uplift

Figure 12 shows the distribution of uplift at the interface between timber and concrete layers. It can be noticed that the uplift at the mid-span were much higher than that at the both ends of the specimen. The maximum timber-concrete uplifts were 0.29 mm, 0.5 mm, and 0.55 mm, recorded for F_1, F_2, and F_3, respectively. The test results showed that the geometrical locking of the connector offered an effective resistance to uplift between concrete and timber layers.

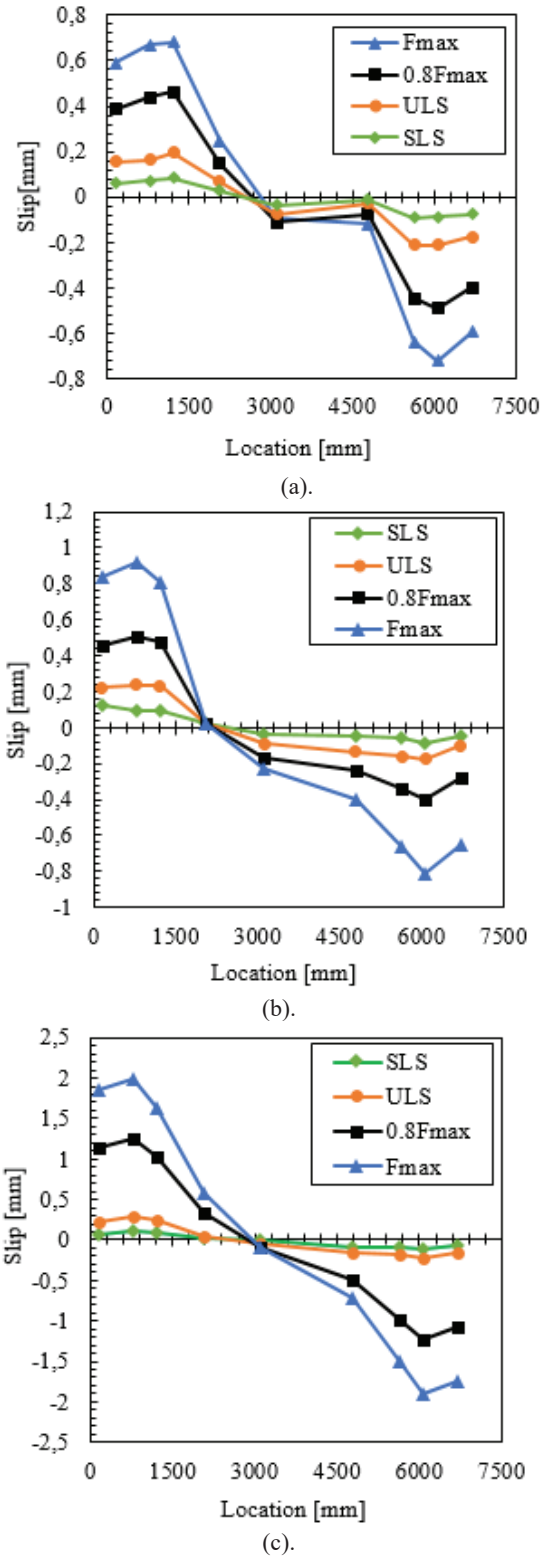

(a). (b). (c).

Figure 11: *Load-slip curves of the composite beams. (a) F_1 test. (b) F_2 test. (c). F_3 test.*

https://doi.org/10.52202/069179-0435

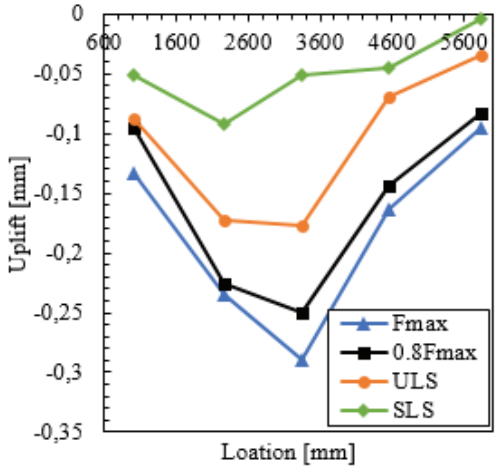

(a).

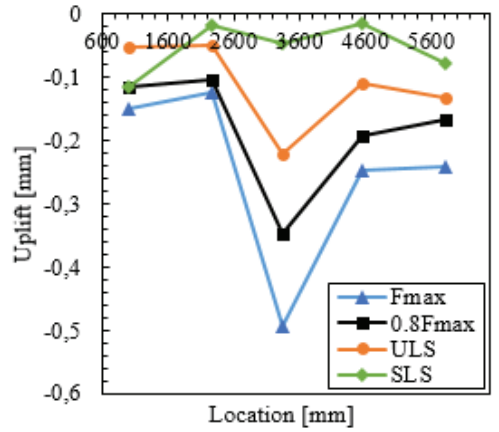

(b).

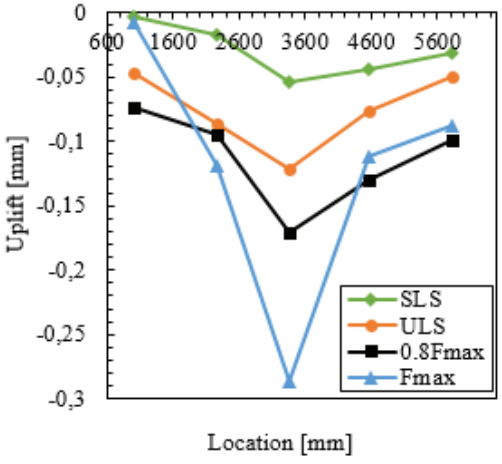

(c).

Figure 12: *Load-uplift curves of the composite beams. (a) F_1 test. (b) F_2 test. (c). F_3 test.*

3.2.5 Analytical evaluation according to Eurocode 5

According to Annex B of the Eurocode 5 guidelines [16], the ϒ-method was employed to assess the flexural performance of the timber-concrete beam. The general effective bending stiffness is expressed as:

$$EI_{eff} = E_1I_1 + E_2I_2 + \gamma_1E_1A_1a_1^2 + \gamma_2E_2A_2a_2^2 \quad (2)$$

For the tested specimens, the Eq.(2) becomes:

$$EI_{eff} = 2(E_1I_1 + E_2I_2 + \gamma_1E_1A_1a_1^2 + \gamma_2E_2A_2a_2^2) \quad (3)$$

In such formula, E_i (MPa), I_i (mm^4), and A_i (mm^2) denote the elastic modulus, the second moment of area, and the cross section of the concrete slab ($i = 1$), and timber beam ($i = 2$), respectively; a_i (mm) represents the distance between the centroid of the component (i) to the overall neutral axis of the composite cross section, given in Eq.(4):

$$a_1 = \frac{\gamma_2E_2A_2}{\sum\gamma_iE_iA_i}d_{1-2}$$

$$a_2 = \frac{\gamma_1E_1A_1}{\sum\gamma_iE_iA_i}d_{1-2} \quad (4)$$

Where, d_{1-2} (mm) is the distance between the centroides of the two components.

Timber was taken as a reference (γ_2=1) and the γ_1 parameter of the shear connector can be written as:

$$\gamma_1 = \frac{1}{1 + \frac{\pi^2A_1E_1s}{KL^2}} \quad (5)$$

Where, K (N/mm) and s (mm) are the stiffness and spacing of shear connectors, respectively, and L (mm) is the beam span.

For the present analytical calculation, the effect of the cracking of concrete is approximated by neglecting the contribution of the concrete drops, except the steel rebars (HA8), while the concrete drops are not taken into account (see Figure 13).

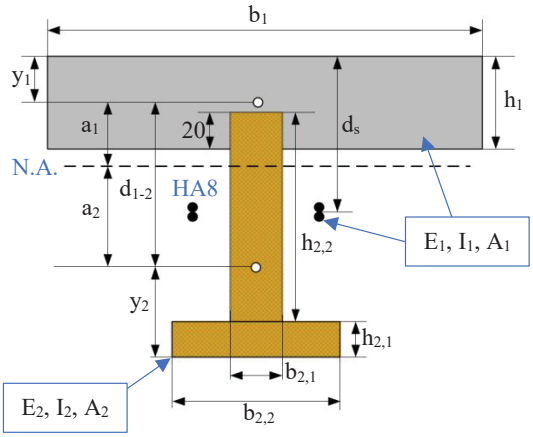

Figure 13: *Composite beam cross section.*

N.A. and d_s denote the overall composite neutral axis and the distance between the steel rebars to the upper slab surface, respectively; and y_i represents the position of the centroid of the element (i).

The geometrical parameters indicated on the Figure 13 were measured and represented in Table 2. While, the

parameters of the analytical method were calculated and provided in Table 3.

Table 2 Dimensions of timber-concrete cross section.

	Parameter	F_1	F_2	F_3
Concrete slab	h_1[mm]	76	83.5	79.5
	b_1[mm]	458.75	457.5	460
	y_1[mm]	41.5	44.1	43.2
	A_1[mm^2]	34875	37982	36614
	I_1[mm^4]	33992832	36126620	37700607
	d_s[mm]	155	159	159.5
Timber beam	$h_{2,1}$[mm]	57.5	59	54.5
	$b_{2,1}$[mm]	68	67.5	68
	$h_{2,2}$[mm]	179	175.5	180
	$b_{2,2}$[mm]	142	140.5	140.5
	y_2[mm]	99.5	98.5	99.4
	A_2[mm^2]	20337	20136	19897
	I_2[mm^4]	103000000	99900000	99700000
	$d_{2,1}$[mm]	151.5	155.4	151.4

Table 3 Effective bending stiffness of test specimens.

	Parameter	F_1	F_2	F_3
	E_1[MPa]	29050	35178	28340
	E_2[MPa]		11166	
	L[mm]		6550	
ELS	K_s[kN/mm]		184.8	
	γ_1	0.65	0.58	0.64
	γ_2		1	
	a_1[mm]	38.8	34.7	37.7
	a_2[mm]	112.7	120.7	113.7
	EI_{eff}[10^{13}Nmm^2]	1.20	1.32	1.20
	EI_{exp}[10^{13}Nmm^2]	1.22	1.57	1.14
	Error (%)	1.6	15.9	5
ELU	K_u[kN/mm]		167.3	
	γ_1	0.63	0.56	0.62
	γ_2		1	
	a_1[mm]	39.9	35.8	38.8
	a_2[mm]	111.6	119.5	112.6
	EI_{eff}[10^{13}Nmm^2]	1.19	1.3	1.19
	EI_{exp}[10^{13}Nmm^2]	1.15	1.49	1.13
	Error (%)	3.3	12.7	5

According to the comparaison results, represented in Table 3, a good accuracy between the analytical and experimental results can be noticed for the specimens F_1 and F_3. Whereas, in case of F_2, the test results were underestimated, at both service and ultimate limit states with an error of 15.9% and 12.7%, respectively.
This approach exhibits an inadequate consideration of concrete cracking, thereby neglecting the beneficial effect of the higher concrete strength in F_2 test on the crack formation.

4 CONCLUSIONS

This paper presents an experimental study on a newly proposed notched connection for timber-concrete composite beams. Three pushout tests were made. The results showed high strength and stiffness of the connector. The high ductility of the connector was obtained as the failure was governed by local crashing of the timber in compression. In order to assess the failure mode, flexural capacity, slip, and uplift of the beam specimens, 6-point bending tests were performed on three timber-concrete specimens. The failure mode was governed by a brittle tensile-flexural rupture of the flange of the timber beam. It must be noted, that after collapse, no failure was observed in either the concrete slab or the notch connectors. The analysis of slips and uplifts revealed the effectiveness of the shear connection without the need of any mechanical elements.
Moreover, the analytical method, proposed in Eurocode 5 guidelines, is used to calculate the effective bending stiffness of the composite beams, with a simple hypothesis to account the concrete cracking. An acceptable accuracy, compared with the experimental results, is reached.
A new methodology, is currently being developed to refine the representation of the concrete cracking in the analytical calculation with the aim of reducing the discrepancy between analytical and test results.

5 REFERENCES

[1] Ministère de la transition écologique et Centre d'études et d'expertise sur les risques, l'environnement, la mobilité et l'aménagement, “Réglementation Environnementale Des Bâtiments Neufs (RE2020),” 2020.

[2] A. Buchanan, Fire performance of timber construction, Prog. Struct. Engng Mater. 2 (2000) 278–289.

[3] A. Dias, Mechanical behaviour of timber-concrete joints, PhD thesis, Technische Universiteit Delft, April 2005.

[4] M; BRANCO, J.S. ; CRUZ et M. PIAZZA : Experimental analysis of laterally loaded nailed timber-to-concrete connections. Construction and Building Materials, 23, 2009.

[5] Bruce L. DEAM, Massimo FRAGIACOMO et Andrew H. BUCHANAN : Connections for composite concrete slab and LVL flooring systems. Materials and Structures, 41(3):495–507, 2008. ISSN 1359-5997.

[6] Ulf Arne GIRHAMMAR : Nail-plates as shear connectors in composite timber and concrete structures. In Congrès de l’AIPC, 1984.

[7] Clouston, P., Bathon, L., and Schreyer, A. (2005). “Shear and bending performance of a novel wood-concrete composite system.” J. Struct. Eng., 131(9), 1404–1412.

[8] Gutkowski R, Brown K, Shigidi A, Natterer J. Laboratory tests of composite woodconcrete beams. Constr Build Mater 2008;22(6):1059−66.

[9] Y. Jiang, X. Hu, W. Hong, J. Zhang, F. He, Experimental study on notched connectors for glulam-lightweight concrete composite beams. BioResources, 15(2020), pp.2171-2180.

[10] AFNOR, NF EN 408 : Bois de structure et bois lamellé-collé, 2012.

[11] CEN. Timber structures – Joints made with mechanical fasteners – General principles for the determination of strength and deformation characteristics, EN 26891: 1991. Brussels; 1991.

https://doi.org/10.52202/069179-0435

[12] Bureau de normalisation (BNETC), XP CEN/TS 19103 Conception et calcul des structures - Calcul des structures mixtes bois-béton - Règles communes et règles pour les bâtiments, BNTEC, 2022.

[13] A. Ceccotti, Structures en bois aux Etats Limites - STEP 2, Chapitre VII-4 : Structures Bois-Béton. Paris : SEDIBOIS / union nationale Française de Charpente, Menuiserie, Parquets, 1997.

[14] S. Fuentes, Flexural test on timber beams, BOIS HD, January 2022.

[15] EN1991-1-1 **:** Eurocode 1 - actions sur les structures - Partie 1-1 : Actions générales — Poids volumiques, poids propres, charges d'exploitation des bâtiments (P 06-111-1:2003-03, NA:2004-06, A1:2009-03).

[16] Eurocode 5, Design of Timber Structures. Part 1-1: General - Common Rules and Rules for Buildings. EN 1995-1-1, Brussels, 2004.